*metals*

MDPI

*Article*

# Microstructure Evolution and Tensile Properties of Medium Manganese Steel Heat Treated by Two-Step Annealing

**Tao Kang [1,2,3,*], Zhanyu Zhan [1], Changcheng Wang [1], Zhengzhi Zhao [2,3], Juhua Liang [4,*] and Lele Yao [1]**

[1] China North Vehicle Research Institute, Beijing 100072, China; 15810075953@163.com (Z.Z.); wccbit@163.com (C.W.); yll1989521@163.com (L.Y.)
[2] Collaborative Innovation Center of Steel Technology, University of Science and Technology Beijing, Beijing 100083, China; zhaozhzhi@ustb.edu.cn
[3] Beijing Laboratory of Metallic Materials and Processing for Modern Transportation, Beijing 100083, China
[4] Key Laboratory of Materials Physics, Institute of Solid State Physics, HFIPS, Chinese Academy of Sciences, Heifei 230031, China
* Correspondence: 13220101686@163.com (T.K.); liangjuhua0721@126.com (J.L.)

**Abstract:** In this paper, the nucleation and growth of austenite are controlled through a two-step annealing process to achieve multi-scale distribution and content increase of retained austenite in low manganese series medium-Mn steel. Combining SEM, EBSD, AES, and other experimental equipment, the evolution rules of the microstructure, properties, and element distribution behavior of the test steel during the annealing process are studied. Compared with one-step annealing, the two-step annealing significantly broadens the size distribution range of retained austenite. In the first step, after annealing at a higher intercritical temperature (760 °C), the ferrite and the M/A island are obtained, completing the initial partition of Mn and the refinement of microstructures. During the second step of annealing (720 °C), the primary Mn-rich martensite region provides higher nucleation driving force and finer dispersed nucleation sites, promoting the nucleation and growth of reverse transformation austenite. At the same time, the metastable-retained austenite formed after the first step of annealing continues to grow through interface movement. Furthermore, a high proportion (23.4%) of retained austenite with multi-scale distribution is formed in the final microstructure, and the product of strength and elongation increased from 21.8 GPa·% by the one-step annealing process to 30.1 GPa·%.

**Keywords:** medium manganese steel; element partition; microstructure; mechanical properties; two-step annealing

check for updates

**Citation:** Kang, T.; Zhan, Z.; Wang, C.; Zhao, Z.; Liang, J.; Yao, L. Microstructure Evolution and Tensile Properties of Medium Manganese Steel Heat Treated by Two-Step Annealing. *Metals* **2024**, *14*, 1008. https://doi.org/10.3390/met14091008

Academic Editor: Koh-ichi Sugimoto

Received: 26 July 2024
Revised: 28 August 2024
Accepted: 29 August 2024
Published: 3 September 2024

**Copyright:** © 2024 by the authors. Licensee MDPI, Basel, Switzerland. This article is an open access article distributed under the terms and conditions of the Creative Commons Attribution (CC BY) license (https://creativecommons.org/licenses/by/4.0/).

## 1. Introduction

In order to adapt to the new era of automobile lightweight development theme of "dual carbon, energy saving, and safety", medium-Mn steel with both high strength and high plasticity has become a highly competitive steel material for future automobiles [1–6]. For cold-rolled medium-Mn steel, its preparation process generally includes softening annealing, cold rolling, and intercritical isothermal annealing [7–12]. Among them, the intercritical annealing temperature and time determine the proportion of retained austenite in the steel [13–15]. At relatively low annealing temperatures, due to the sufficient enrichment of C and Mn elements, intercritical austenite often has high thermodynamic stability and remains at room temperature after cooling. However, since the reverse transformation rate of austenite at low temperature is very slow, it often takes several hours or even dozens of hours to obtain a certain amount of retained austenite [16]. When intercritical annealing at higher temperature, although the reverse transformation rate of austenite is accelerated, the stability of the intercritical austenite is significantly reduced, and part of the austenite inevitably transforms into quenched martensite during the cooling process. Therefore, a suitable intercritical annealing process needs to be designed to balance the effects of

annealing temperature and annealing time on austenite. Liang et al. [17] improved the uniformity of the microstructure and optimized the comprehensive mechanical properties of the material by introducing a pre-quenching process before intercritical annealing. Hu et al. [18] increased the reverse transformation kinetics of austenite by pre-precipitating cementite particles of different sizes before intercritical annealing and finally obtained the largest proportion of retained austenite and the product of strength and elongation. Ding et al. [19] introduced pre-austenite structure into the steel through complete austenitization quenching before intercritical annealing, thereby accelerating the phase transformation kinetics of austenite during intercritical annealing.

Drawing on the above process design ideas, this paper designed an intercritical two-step annealing process and systematically studied the microstructure morphology characteristics, element distribution behavior, and mechanical property changes of medium-Mn steel under different annealing processes.

## 2. Experimental Procedures

The chemical composition of the experimental steel is 0.23C-0.97Si-3.48Mn-0.96Al-0.15V-0.18Mo-0.021P-0.003S (wt.%). A 50 kg ingot was hot forged into a rectangular forging billet with a cross-sectional area of 70 × 100 $mm^2$. It was heated at 1200 °C for 1 h and then rolled to a thickness of 3.6 mm in six passes and air-cooled to room temperature. The hot-rolled plate was isothermally treated at 600 °C for 1.5 h and water-cooled to room temperature (named as A-600). After pickling and cold rolling, a rectangular sample with a size of 2.6 × 100 × 20 $mm^3$ was cut from the cold-rolled plate along the rolling direction and placed in an SX2-16-13 box-type resistance furnace. This paper designed two heat treatment processes for cold-rolled specimens, as shown in Figure 1. Among them, the blue dashed line is the one-step annealing process route, and the black solid line is the two-step annealing process route, named one-step and two-step, respectively. The phase fraction of the experimental steel at different temperatures was calculated using the Thermocal-Calc thermodynamics software based on the TCFE10 database, as shown in Figure 2. According to the phase diagram, 700, 720, and 760 °C were selected as the intercritical austenitization temperatures of the one-step annealing process and were named CR-700, CR-720, and CR-760, respectively. For two-step annealing, 760 °C was selected as the first-step annealing temperature, and 700 and 720 °C were selected as the second-step annealing temperatures and were named 760-700 and 760-720, respectively. In addition, for both heat treatment processes (one-step and two-step), the heat treatment time at different austenitizing temperatures was set to 10 min.

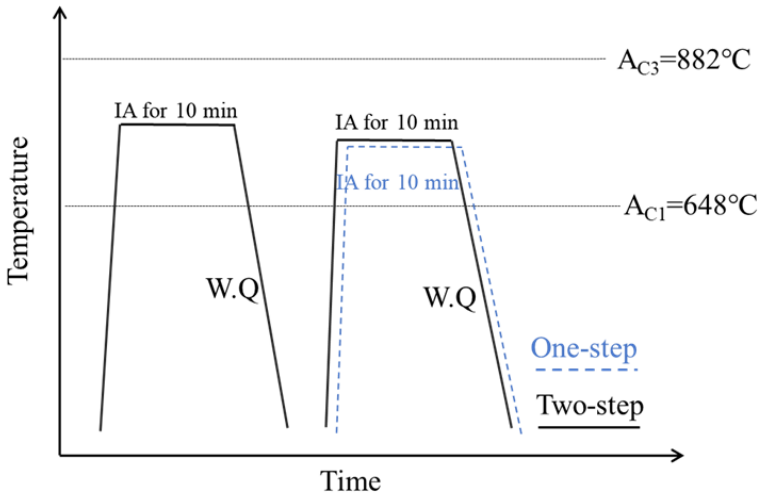



**Figure 1.** Schematic diagram of heat treatment process. IA and W.Q denote the intercritical annealing and water quenching, respectively.

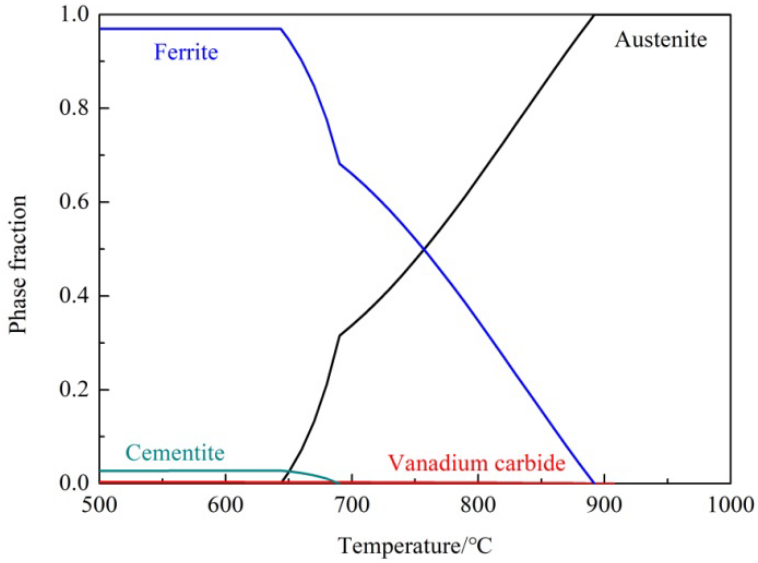



**Figure 2.** Phase fraction as a function of temperature.

Tensile properties were obtained using uniaxial tensile testing performed at a crosshead speed of 1 mm/min and a gauge length of 25 mm. After the sample was polished and etched with 2% nitric acid alcohol, its microstructure was observed using a Zeiss 55 scanning electron microscope (manufacturer's name, city location, country). Thin foil samples (G20) for TEM observation were prepared using the double-jet polishing technique (5% perchlorate alcohol at −30 °C, applied potential of 50 V). After mechanical grinding, the sample was electropolished in an electrolyte composed of 10% perchloric acid and 90% ethanol to remove residual stress on the surface. The voltage was controlled at 15 V, the current was 1.5 A, and the polishing was continued for 12 s. The PHI-710 Auger (manufacturer's name, city location, country) nanoelectron probe equipped with electron backscatter diffraction was used to characterize the microscopic morphology of each component phase in the steel with an acceleration voltage of 20 kV and a step size of 0.04 μm. Finally, EDAX-OIM software was used to process the EBSD raw data. In addition, AES line scan analysis was used to detect the distribution of Mn elements in selected areas of the CR-760.

## 3. Results and Discussion

### *3.1. Microstructure Analysis*

The SEM micrographs of typical samples are shown in Figure 3. The hot-rolled martensite in the A-600 is tempered, and large-sized cementite particles are uniformly dispersed and precipitated at the martensite lath interface and within the lath. The final room-temperature microstructure is composed of ferrite and cementite (Figure 3b). After cold rolling and one-step annealing, reverse-transformed austenite begins to nucleate at the interface between ferrite and cementite. The cementite continues to dissolve and provide carbon and manganese elements for austenite, and austenite continues to grow through interface movement. The CR-720 is ultimately composed of austenite, ferrite, and a small amount of cementite (Figure 3b). For the CR-760, due to the excessively high annealing temperature, the stability of intercritical austenite is greatly reduced, resulting in a large amount of austenite transforming into quenched martensite during the cooling process (Figure 3c). After two-step annealing, the microstructure of the 760-720 is composed of ferrite and austenite. In addition, island-like tissue divided by "thin lines" appeared in the 760-720, as shown in the red rectangular area in Figure 3d.

TEM technology was used to characterize the island microstructure in the 760-720, and the results are shown in Figure 4. By calibrating the diffraction pattern at the position shown in the white circle in Figure 4a, the result shows that its crystal structure is face-centered cubic, indicating that the phase is retained austenite with a face-centered cubic

structure, and the "fine linear" microstructure located in the middle of the lath austenite is intercritical ferrite with a body-centered cubic structure, which is consistent with the observation results in SEM. In addition, the interior of the ferrite is very pure and there is no tangle of dislocations.

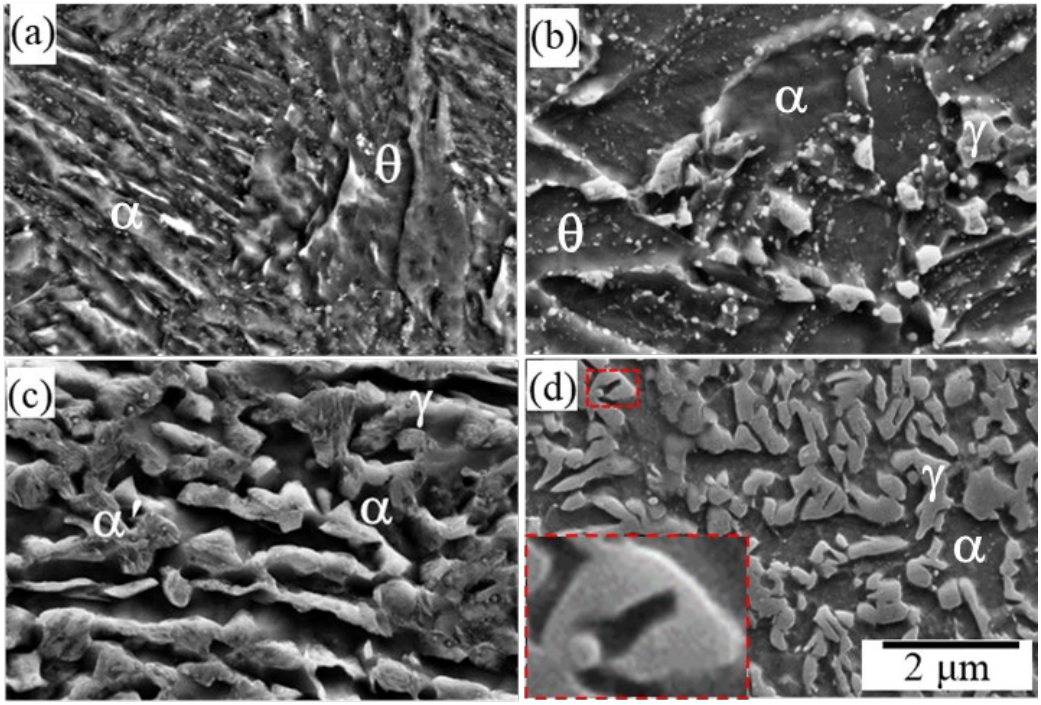



**Figure 3.** SEM micrographs of typical samples. (**a**) A-600; (**b**) CR-720; (**c**) CR-760; (**d**) 760-720. The α, γ, α′, and θ represent ferrite, austenite, martensite, and cementite, respectively.

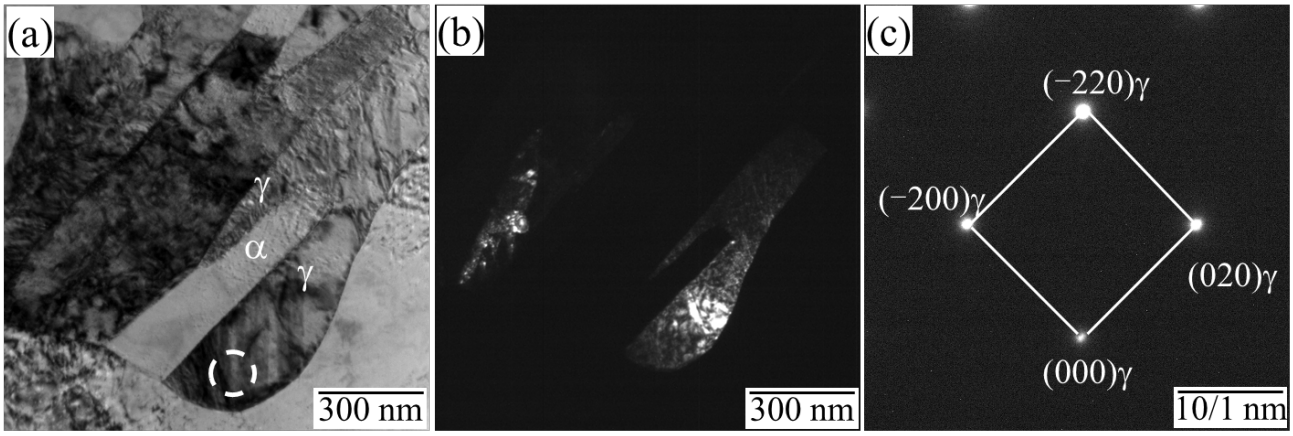



**Figure 4.** TEM microstructure characterization of 760-720: (**a**) bright field image; (**b**) dark field image; (**c**) diffraction pattern marked by the white circle in (**a**).

### *3.2. Analysis of Element Partition and Austenite Characteristics*

Analysis suggests that the formation of the "thin linear" microstructure in the 760-720 is closely related to the initial microstructure before the second-step of intercritical annealing. Therefore, Electron Back-Scattered Diffraction (EBSD) and Auger Electron Spectroscopy (AES) technology were combined to detect the microstructure composition of the CR-760 and the distribution of Mn between different phases. The results are shown in Figure 5.

Figure 5a shows the EBSD microstructure characterization of the CR-760. The retained austenite is coded in red, the ferrite is coded in gray, and the martensite has poor contrast

due to its high dislocation density and is coded in black or dark gray [20]. Figure 5b is an enlarged contrast diagram of the white rectangular area in Figure 5a. The red dotted line in the figure is the line scan area of the Auger nanoprobe. According to the line scan results of the Auger nanoprobe in Figure 5c, it can be seen that the intensity of Mn concentration in martensite is significantly higher than that of ferrite. This is because during the intercritical annealing process of the CR-760, the diffusion of Mn element from the ferrite to the austenite occurred, causing complete manganese enrichment in austenite, and the martensite inherited the Mn content in the intercritical austenite, while ferrite becomes a Mn-poor phase that remains at room temperature. In addition, the intensity of Mn concentration at the martensite interface is significantly higher than that within its grains. During the intercritical isothermal process, the Mn element tends to be enriched preferentially at the austenite interface. Due to the short annealing time, the Mn element cannot be fully homogenized within the austenite grains, so the intercritical austenite interface has a higher Mn content. After the sample is quenched, the martensite inherits the distribution characteristics of the Mn element in the intercritical austenite, which ultimately manifests as a higher Mn content at the martensite interface. During the second step of intercritical annealing, reverse-transformed austenite nucleates at the Mn-rich martensite interface and grows along the interface, while the Mn-poor region in the center of the martensite grain eventually forms the intercritical ferrite.

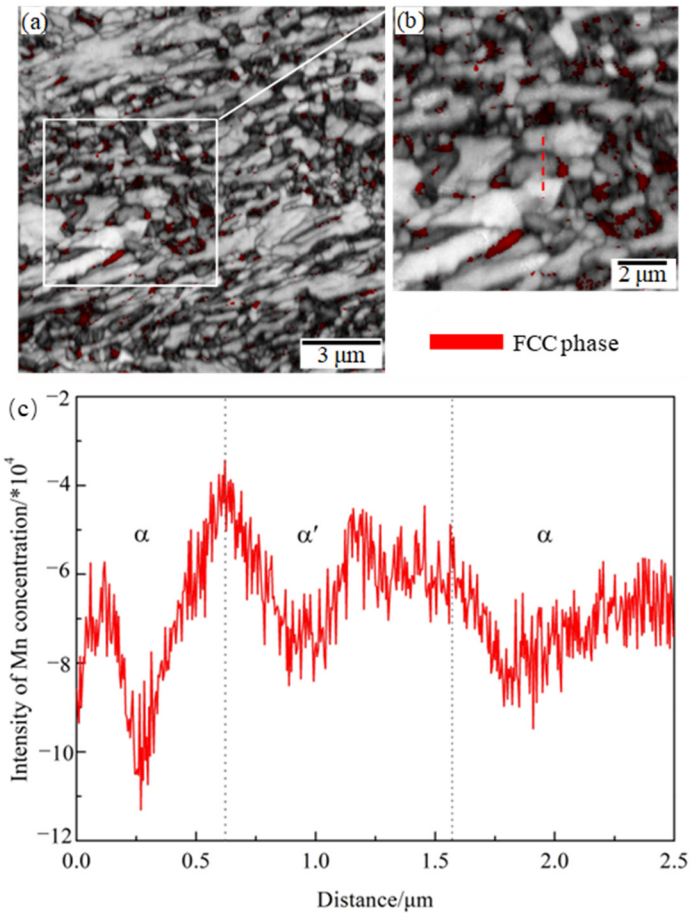



**Figure 5.** EBSD characterization of CR-760 (**a**); (**b**) an enlarged view of the area corresponding to the white rectangle in (**a**); (**c**) intensity of Mn element measured along the red line in (**b**).

Figure 6 shows the EBSD characterization of one-step annealing and two-step annealing samples. Figure 6a compared with the CR-700. Due to the increase in annealing temperature, the proportion of retained austenite in the CR-720 significantly increases to 11.5%, and adjacent austenite grows into larger grains by merging. For the two-step

specimen, as the austenitization temperature increases, the proportion of retained austenite increases from 12.4% in the 760-700 to 23.4% in the 760-720. Figure 6c,f shows the KAM images of ferrite in CR-720 and 760-720. According to statistics, the average KAM value of the former BCC phase is 0.67, while the KAM value of the latter BCC phase is only 0.53, indicating that the former has a higher dislocation density in the ferrite.

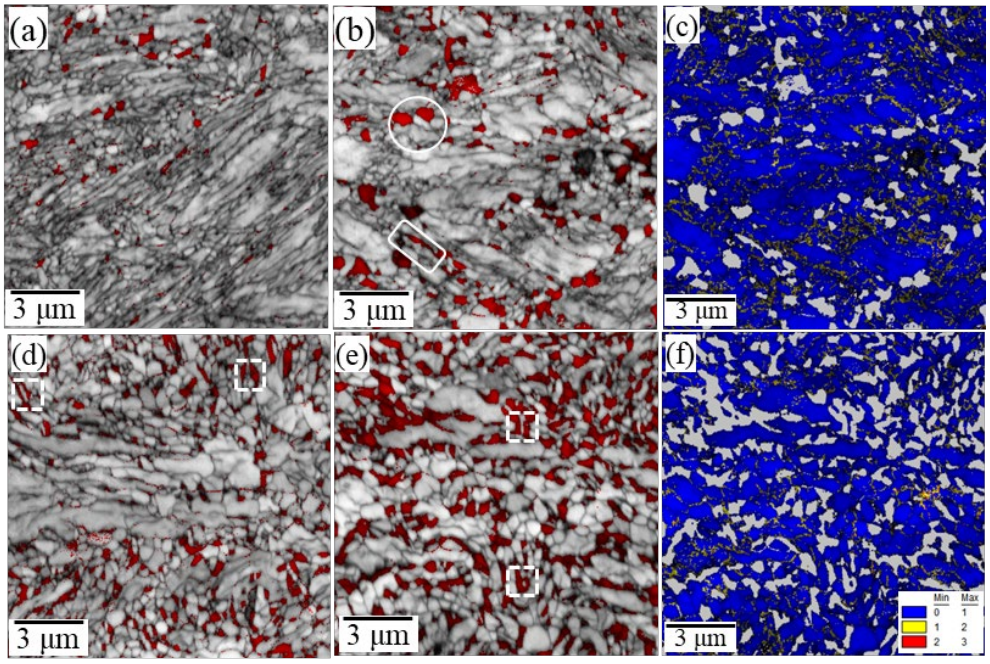



**Figure 6.** EBSD image quality maps with phase maps marking retained austenite in red (**a**,**b**,**d**,**e**) and KAM maps of BCC structures (**c**,**f**) of different samples: (**a**) CR-700; (**b**,**c**) CR-720; (**d**) 760-700; (**e**,**f**) 760-720.

The grain size distribution of retained austenite in CR-720 and 760-720 (equivalent to a circle) is shown in Figure 7. It can be seen that compared with the CR-720, there is a higher proportion of grains with sizes above 0.5 μm in the 760-720 sample, and retained austenite of different sizes can produce a sustained TRIP effect during the plastic deformation process, thereby improving the mechanical properties of the material.

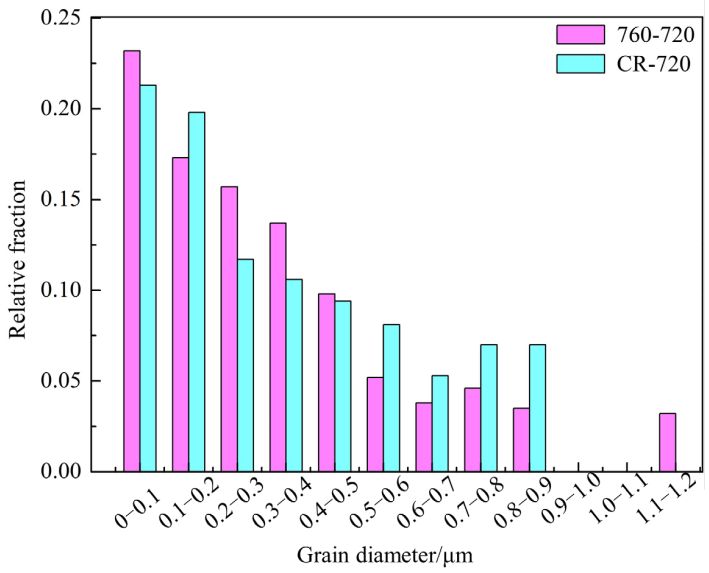



**Figure 7.** Grain size distribution of retained austenite in CR-720 and 760-720.

### *3.3. Analyses of Mechanical Properties*

The engineering stress-strain curve of the test steel is shown in Figure 8, and the detailed mechanical properties are shown in Table 1. It can be seen that as the intercritical austenitization temperature increases, the yield strength of the one-step annealed specimen decreases, and the tensile strength and total elongation increase. Among them, the yield strength is mainly related to the dislocation strengthening, fine grain strengthening, and solid solution strengthening of the alloy elements in the ferrite. As the austenitization temperature increases, the proportion of distortion-free equiaxed ferrite in the sample increases, which reduces the dislocation density in the ferrite and weakens the dislocation strengthening effect [21]. In addition, as the temperature increases, the alloying elements in the ferrite continue to diffuse into the austenite, causing the solid solution strengthening effect in the ferrite to weaken and the yield strength to decrease [22]. At the same time, the equiaxed grains continue to merge and grow, and the strengthening effect of fine grains is weakened, resulting in a decrease in the yield strength. The tensile strength is related to the proportion of intercritical austenite in the sample. The greater the proportion of intercritical austenite, the more it will transform into a higher proportion of strain-induced martensite after plastic deformation, improving the tensile strength of the material. The total elongation is related to the proportion of retained austenite, and the higher proportion of retained austenite in CR-720 results in a greater total elongation.

**Table 1.** Tensile properties and retained austenite values of one-step and two-step samples.

| Sample | YS/MPa | TS/MPa | TE/% | TS × E/GPa·% | RA Values/% |
|---|---|---|---|---|---|
| CR-700 | 942 | 1011 | 15.3 | 15.5 | 3.4 |
| CR-720 | 870 | 1118 | 19.5 | 21.8 | 11.5 |
| 760-700 | 867 | 1052 | 25.9 | 27.2 | 12.4 |
| 760-720 | 735 | 1189 | 25.3 | 30.1 | 23.4 |

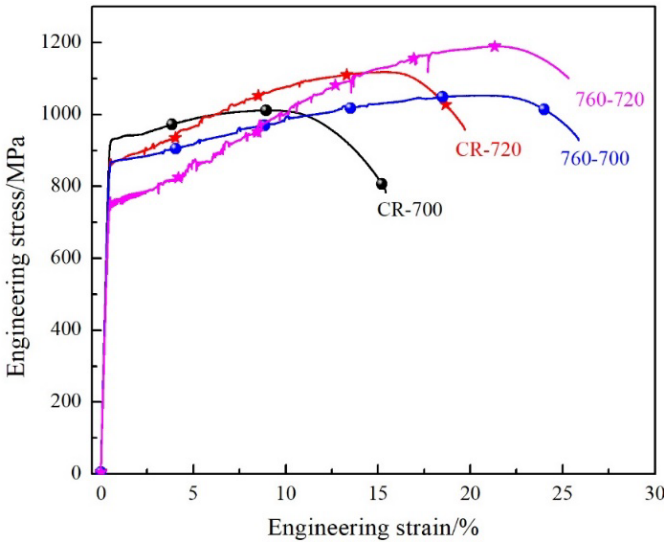



**Figure 8.** The engineering stress-strain curves of different samples.

Compared with CR-720, the 760-720 sample after two-step annealing has higher total elongation and product of strength and elongation. The tensile strength increases slightly, and the yield strength decreases. The difference in yield strength between the two is related to the dislocation density in the ferrite. According to the KAM analysis results, it can be seen that the ferrite dislocation density in 760-720 is low. During the plastic deformation process, the movable dislocations begin to slip under low applied stress, which significantly reduces the yield strength of the specimen.

Analysis suggests that the difference in the proportion and size distribution of retained austenite in CR-720 and 760-720 is related to the initial microstructure before intercritical annealing. Since the 760-720 formed a large amount of Mn-rich martensite after the first step of intercritical annealing, it promoted the nucleation and growth of reverse-transformed austenite during the second step of intercritical annealing [23].

Figure 9 is a schematic diagram of the microstructure evolution of the 760-720 sample during the two-step intercritical annealing process. During the first step of intercritical austenitization of the sample, due to the higher annealing temperature, the diffusion rate of elements is faster, and intercritical austenite with different grain sizes is formed in a short isothermal process, as shown in Figure 9a. During the first step of intercritical austenitizing and quenching of the sample, due to the different enrichment degrees of elements in the intercritical austenite with different grain sizes, different degrees of martensitic transformation occurred. Among them, the following is noticed: The Mn-poor region in the first type of austenite undergoes martensitic phase transformation, while the areas with higher alloying element enrichment such as the austenite grain boundaries do not undergo martensitic phase transformation and eventually remain at room temperature; the second type of austenite is completely transformed into martensite during the quenching process due to its lower stability; the third type of austenite is retained at room temperature due to its high thermodynamic stability, as shown in Figure 9b. Among them, the quenched martensite inherits the Mn content of the intercritical austenite, forming a Mn-rich martensite phase.

During the second step of intercritical annealing, the phase transformation behavior of the above three types of austenite is shown in Figure 9c. Among them, the following is noticed: The interface of the first type of austenite continuously moves toward the adjacent ferrite, and is accompanied by the diffusion and distribution of carbon and manganese elements in ferrite into austenite, promoting the rapid growth of austenite; the alloying elements are fully enriched at the martensite lath interface formed by the complete transformation of the second type of austenite, which promotes the rapid nucleation of reverse-transformed austenite and its gradual growth along the martensite interface; the third type of austenite does not nucleate during the second step of intercritical annealing, but only grows through interface movement. At the same time, the carbon and manganese elements in the surrounding microstructure continue to diffuse and distribute into the austenite, promoting the rapid growth of austenite along the martensite interface [24]. During the second step of intercritical austenitizing and quenching, the stability of the first and third types of austenite is further improved due to the secondary enrichment of carbon and manganese elements, and finally, all are retained at room temperature. The second type of austenite has higher thermodynamic stability due to its smaller grain size, does not undergo martensite transformation during the cooling process, and remains at room temperature.

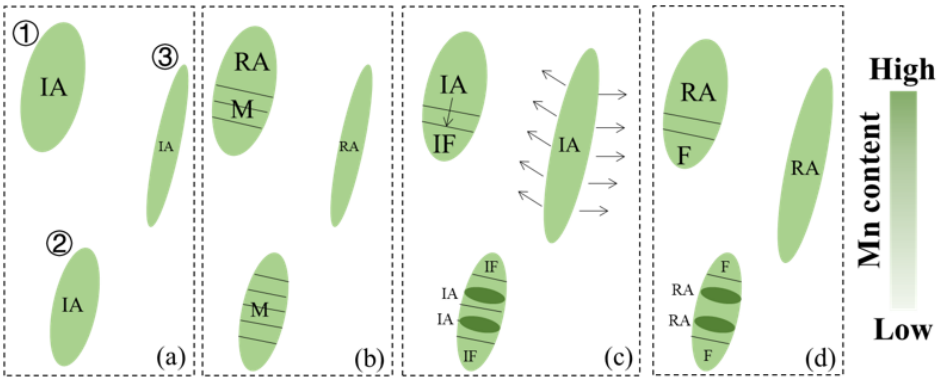



**Figure 9.** Schematic diagram of microstructure evolution during two-step annealing process of 760-720 (IA, intercritical austenite; RA, retained austenite; M, quenched martensite; IF, intercritical ferrite; F, ferrite): (**a**) during the first step annealing process; (**b**) after the first step annealing is completed; (**c**) during the second step annealing process; (**d**) after the second step annealing is completed. The ①, ②, and ③ represent the first, second, and third types of austenite, respectively.

In summary, the austenite reverse transformation behavior of the 760-720 during the second step of intercritical annealing can be divided into two categories: (1) The pre-existing austenite continues to grow directly through the movement of the interface, significantly reducing the driving force required for austenite reverse transformation; (2) The newly nucleated reverse-transformed austenite gradually grows along the martensite interface, and the Mn-rich martensite provides an additional driving force for the nucleation and growth of reverse-transformed austenite [25].

## 4. Conclusions

This paper takes low manganese series medium-Mn steel as the research object, clarifies the impact of the two-step intercritical annealing process on the microstructure and mechanical properties of the experimental steel, and draws the following conclusions:

1. After the first step of higher temperature annealing, the 760-720 obtains the microstructure of ferrite and M/A island, achieving the preliminary distribution of manganese elements and the refinement of the microstructure. During the second annealing process, the Mn-rich martensite provides higher nucleation driving force and finer dispersed nucleation sites for the reverse-transformed austenite. At the same time, the metastable austenite formed after the first step of annealing continues to grow through interface movement, and a high proportion (23.4%) of retained austenite with multi-scale distribution is formed in the final microstructure.
2. Compared with the CR-720, the high proportion of multi-scale retained austenite in the 760-720 significantly increases the total elongation and TS × E of the material, while the lower dislocation density within ferrite grains results in a reduction in its yield strength. The 760-720 shows better and excellent mechanical properties, with a tensile strength of 1189 MPa, a total elongation of 25.3%, and a product of strength and elongation of 30.1 GPa%.

**Author Contributions:** Conceptualization, T.K. and Z.Z. (Zhanyu Zhan); methodology, Z.Z. (Zhanyu Zhan) and J.L.; software, T.K. and Z.Z. (Zhanyu Zhan); validation, Z.Z. (Zhanyu Zhan) and C.W.; formal analysis, J.L. and Z.Z. (Zhengzhi Zhao); investigation, Z.Z. (Zhanyu Zhan) and C.W.; resources, J.L. and Z.Z. (Zhengzhi Zhao); data curation, T.K.; writing—original draft preparation, T.K.; writing—review and editing, J.L. and L.Y.; visualization, Z.Z. (Zhanyu Zhan) and L.Y.; supervision, C.W. and L.Y.; project administration, Z.Z. (Zhengzhi Zhao); funding acquisition, Z.Z. (Zhengzhi Zhao) and J.L. All authors have read and agreed to the published version of the manuscript.

**Funding:** This research was funded by key research and development plan of Shandong Province (grant number 2019TSLH0103) and the National Natural Science Foundation of China (grant number 52001304).

**Data Availability Statement:** The data that support the findings of this study are available from the corresponding authors upon reasonable request.

**Conflicts of Interest:** The authors declare no conflicts of interest.

## References

1. Yan, S.; Liang, T.; Chen, J.; Li, T.; Liu, X. A novel Cu-Ni added medium Mn steel: Precipitation of Cu-rich particles and austenite reversed transformation occurring simultaneously during ART annealing. *Mater. Sci. Eng. A* **2019**, *746*, 73–81. [CrossRef]
2. Park, G.; Kim, K.; Uhm, S.; Lee, C. A comparison of cross-tension properties and fracture behavior between similar and dissimilar resistance spot-weldments in medium-Mn TRIP steel. *Mater. Sci. Eng. A* **2019**, *752*, 206–216. [CrossRef]
3. Liu, C.; Peng, Q.; Xue, Z.; Deng, M.; Wang, S.; Yang, C. Microstructure-tensile properties relationship and austenite stability of a Nb-Mo micro-alloyed medium-Mn TRIP steel. *Metals* **2018**, *8*, 615. [CrossRef]
4. Niu, G.; Wu, H.; Zhang, D.; Gong, N.; Tang, D. Heterogeneous nano/ultrafine-grained medium Mn austenitic stainless steel with high strength and ductility. *Mater. Sci. Eng. A* **2018**, *725*, 187–195. [CrossRef]
5. Shao, C.; Hui, W.; Zhang, Y.; Zhao, X.; Weng, Y. Effect of intercritical annealing time on hydrogen embrittlement of warm-rolled medium Mn steel. *Mater. Sci. Eng. A* **2018**, *726*, 320–331. [CrossRef]
6. Liu, C.; Peng, Q.; Xue, Z.; Wang, S.; Yang, C. Microstructure and mechanical properties of hot-rolled and cold-rolled medium-Mn TRIP steels. *Materials* **2018**, *11*, 2242. [CrossRef]

7. Shi, J.; Hu, J.; Wang, C.; Wang, C.-Y.; Dong, H.; Cao, W.-Q. Ultrafine grained duplex structure developed by ART-annealing in cold rolled medium-Mn steels. *J. Iron Steel Res. Int.* **2014**, *21*, 208–214. [CrossRef]
8. Zhao, C.; Zhang, C.; Cao, W.-Q.; Yang, Z.-G. Variation in retained austenite content and mechanical properties of 0.2C–7Mn steel after intercritical annealing. *Int. J. Miner. Metall. Mater.* **2016**, *23*, 161–167. [CrossRef]
9. Hu, Z.P.; Xu, Y.B.; Zou, Y.; Misra, R.D.K.; Han, D.T.; Chen, S.Q.; Hou, D.Y. Effect of intercritical rolling temperature on microstructure-mechanical property relationship in a medium Mn-TRIP steel containing δ ferrite. *Mater. Sci. Eng. A* **2018**, *720*, 1–10. [CrossRef]
10. Kwok, T.W.J.; Gong, P.; Xu, X.; Nutter, J.; Rainforth, W.M.; Dye, D. Microstructure evolution and tensile behaviour of a cold rolled 8 Wt% Mn medium manganese Steel. *Metall. Mater. Trans. A* **2022**, *53*, 597–609. [CrossRef]
11. Bansal, G.K.; Madhukar, D.A.; Chandan, A.K.; Ashok, K.; Mandal, G.K.; Srivastava, V.C. On the intercritical annealing parameters and ensuing mechanical properties of low-carbon medium-Mn steel. *Mater. Sci. Eng. A* **2018**, *733*, 246–256. [CrossRef]
12. Yang, F.; Luo, H.; Pu, E.; Zhang, S.; Dong, H. On the characteristics of Portevin–Le Chatelier bands in cold-rolled 7Mn steel showing transformation-induced plasticity. *Int. J. Plast.* **2018**, *103*, 188–202. [CrossRef]
13. Kim, D.H.; Kang, J.H.; Ryu, J.H.; Kim, S.J. Effect of austenitization of cold-rolled 10 wt% Mn steel on microstructure and discontinuous yielding. *Mater. Sci. Eng. A* **2020**, *774*, 138930. [CrossRef]
14. Han, J.; Lee, Y.-K. The effects of the heating rate on the reverse transformation mechanism and the phase stability of reverted austenite in medium Mn steels. *Acta Mater.* **2014**, *67*, 354–361. [CrossRef]
15. Bai, S.; Xiao, W.; Niu, W.; Li, D.; Liang, W. Microstructure and mechanical properties of a medium-Mn steel with 1.3 GPa-strength and 40%-ductility. *Materials* **2021**, *14*, 2233. [CrossRef]
16. Arlazarov, A.; Gouné, M.; Bouaziz, O.; Hazotte, A.; Petitgand, G.; Barges, P. Evolution of microstructure and mechanical properties of medium Mn steels during double annealing. *Mater. Sci. Eng. A* **2012**, *542*, 31–39. [CrossRef]
17. Liang, J.; Zhao, Z.; Tang, D.; Ye, N.; Yang, S.; Liu, W. Improved microstructural homogeneity and mechanical property of medium manganese steel with Mn segregation banding by alternating lath matrix. *Mater. Sci. Eng. A* **2018**, *711*, 175–181. [CrossRef]
18. Hu, B.; Luo, H. A novel two-step intercritical annealing process to improve mechanical properties of medium Mn steel. *Acta Mater.* **2019**, *176*, 250–263. [CrossRef]
19. Hahn, G.T. A model for yielding with special reference to the yield-point phenomena of iron and related bcc metals. *Acta Metall.* **1962**, *10*, 727–738. [CrossRef]
20. Gao, F.; Gao, Z.; Zhu, Q.; Yu, F.; Liu, Z. Deformation behavior of retained austenite and its effect on plasticity based on in-situ EBSD analysis for transformable ferritic stainless steel. *J. Mater. Res. Technol.* **2022**, *20*, 1976–1992. [CrossRef]
21. Xu, H.; Han, C.; Bai, Y.; Qiao, X.; Liu, W.; Li, W.; Sha, X. Effect of deformation amount distribution in the austenite recrystallization temperature region on the microstructure and mechanical properties of the X70 pipeline steel. *Ironmak. Steelmak.* **2023**, *50*, 402–409. [CrossRef]
22. Chung, H.; Kim, D.W.; Cho, W.J.; Han, H.N.; Ikeda, Y.; Ishibashi, S.; Körmann, F.; Sohn, S.S. Effect of solid-solution strengthening on deformation mechanisms and strain hardening in medium-entropy V1-xCrxCoNi alloys. *J. Mater. Sci. Technol.* **2022**, *108*, 270–280. [CrossRef]
23. Xie, Z.J.; Yuan, S.F.; Zhou, W.H.; Yang, J.R.; Guo, H.; Shang, C.J. Stabilization of retained austenite by the two-step intercritical heat treatment and its effect on the toughness of a low alloyed steel. *Mater. Des.* **2014**, *59*, 193–198. [CrossRef]
24. Zhu, J.; Ding, R.; He, J.; Yang, Z.; Zhang, C.; Chen, H. A cyclic austenite reversion treatment for stabilizing austenite in the medium manganese steels. *Scr. Mater.* **2017**, *136*, 6–10. [CrossRef]
25. Sugimoto, K.I.; Kobayashi, M.; Hashimoto, S.I. Ductility and strain-induced transformation in a high-strength transformation-induced plasticity-aided dual-phase steel. *Metall. Trans. A* **1992**, *23*, 3085–3091. [CrossRef]


**Disclaimer/Publisher's Note:** The statements, opinions and data contained in all publications are solely those of the individual author(s) and contributor(s) and not of MDPI and/or the editor(s). MDPI and/or the editor(s) disclaim responsibility for any injury to people or property resulting from any ideas, methods, instructions or products referred to in the content.